Single cerium zirconate buffer layer on biaxially textured metal substrates for high performance coated conductors

**Jie Xiong · Wenfeng Qin · Miao Yu ·
Bowan Tao · Ning Zhang · Fei Zhang ·
Xiao Feng · Xiaoke Song · Yanrong Li**

Abstract Textured cerium zirconate ($Ce_xZr_{1-x}O_2$) films were deposited on biaxially textured Ni-5at.%W substrate by direct-current (dc) reactive magnetron sputtering for low cost production of high performance $YBa_2Cu_3O_{7-\delta}$ (YBCO) coated conductors. Film composition was controlled by modulating dc power applied to the Ce metal target. X-ray diffraction analysis shows that all the samples exhibit epitaxial growth, with c-axis perpendicular to the substrate surface. The YBCO film deposited directly on the $Ce_{0.32}Zr_{0.68}O_2$ layer for optimized lattice matching shows a transition temperature T_c and critical current density J_c (75.5 K, self field) of 90.4 K and 1.3 MA/cm^2. The in-field dependence of J_c is similar to the standard CeO_2/YSZ/ CeO_2 buffered samples. These results demonstrate that a single $Ce_xZr_{1-x}O_2$ buffer layer, instead of CeO_2/YSZ/CeO_2 multi-buffer layers for the fabrication of YBCO coated conductors, provides advantages such as simplified architecture and potentially reduced cost due to the reduced fabrication steps.

J. Xiong (✉) · M. Yu · B. Tao · N. Zhang · F. Zhang ·
X. Feng · X. Song · Y. Li
State Key Laboratory of Electronic Thin Film and Integrated
Devices, University of Electronic Science and Technology
of China, Chengdu 610054, People's Republic of China
e-mail: bearbear622@163.com

J. Xiong
Division of Materials Physics and Applications, Los Alamos
National Laboratory, Los Alamos, NM 87545, USA

W. Qin
Civil Aviation Engineer Institute, Civil Aviation Flight
University of China, Guanghan 618307,
People's Republic of China

Introduction

$YBa_2Cu_3O_{7-\delta}$ (YBCO) coated conductors (CCs) have received increased attention from researchers worldwide, due to their lower ac loses, better in-field performance, and lower processing costs compared with first-generation high-temperature superconductor wires [1–3]. In order to successfully develop CCs for practical applications, it is necessary to suppress the interdiffusion, reduce lattice mismatch between YBCO and bare metal substrates, and improve the overall crystallographic texture in the YBCO layer. To fabricate YBCO films with high current carrying capability on textured metal substrate, typical tri-layer stacks of CeO_2/YSZ/CeO_2 or CeO_2/YSZ/Y_2O_3 are the most commonly explored architectures, i.e., CeO_2 (or Y_2O_3) film is used as a seed layer and cap layer, while YSZ plays a major role of diffusion barrier [4, 5]. However, some challenges such as process complexity and high manufacturing cost are still present. It should be noted that a single buffer architecture has been developed recently, such as Y_2O_3 [6, 7], $La_2Zr_2O_7$ [8], $LaMnO_3$ [9, 10], and $SrTiO_3$ [11]. As a promising candidate of buffer material for YBCO CCs, CeO_2 film development has been attempted by many groups due to its excellent chemical compatibility with Ni-based alloy substrates as well as good lattice match with YBCO or ReBCO (Re = Rare earth element). Unfortunately, due to the existence of a critical thickness of ~ 50 nm, beyond which cracks are known to form and micro-cracks propagate, CeO_2 has seldom been successfully used as a single buffer layer [12, 13]. Alternatively, the use of Zr-doped CeO_2 allows for a very thick and crack-free $Ce_xZr_{1-x}O_2$ (CZO) layer, making it possible to combine the previously stated functions into one layer and replace the tri-layer of CeO_2/ YSZ/CeO_2.

In this study, we report epitaxial CZO films with adjustable lattice constants for better lattice matching as a single buffer layer for YBCO CCs. The growth of subsequent YBCO films on this optimized single platform is also investigated.

Experimental

Deposition of CZO thin films ($\sim$0.3 μm thick) was performed by direct-current (dc) reactive magnetron sputtering with the two sputtering guns arranged symmetrically with respect to the substrate, one with a Ce (99.99%) target and the other with a Zr (99.95%) target. The short substrates cut from a 10 m long Ni-5at.%W (NiW) tape were manufactured and supplied by evico GmbH with a thickness of 70 μm and width of 10 mm. The substrate was heated to 750 °C at forming gas pressure (96%Ar + 4%H$_2$) of 2.0 Pa. Water vapor was introduced inside the chamber near the NiW substrates at a pressure of 10^{-3} Pa to react with deposited Cerium and Zirconium atoms. In order to grow CZO films with different Ce concentration, the dc power applied to the Zr target was kept constant at 100 W, while the dc power applied to the Ce target was varied from 30 to 100 W. YBCO films with a thickness of about 0.54 μm were deposited by dc sputtering on short segments of the buffered substrates. Details of the experimental conditions were reported elsewhere [14, 15].

X-ray diffraction analysis (θ–2θ, ω-scan, and ϕ-scan) was used to characterize the structure, texture, and lattice parameter of CZO and YBCO films. The composition of CZO was determined by energy dispersive spectroscopy (EDS). Surface morphology was examined by atomic force microscopy (AFM tapping mode). Secondary ion mass spectrometer (SIMS) analysis was carried out to evaluate the effectiveness of buffer architecture as a barrier against interdiffusion. A four-probe technique with a 1 μV/cm voltage criterion was used to measure superconducting properties, i.e., transition temperature (T_c) and critical current density (J_c) at 75.5 K. The angular dependence of J_c was measured in the maximum Lorentz force configuration at 75.5 K and a 1 T magnetic field.

Results and discussion

The epitaxial nature of CZO films with various compositions was investigated using XRD, indicating all the films were good epitaxial with c-axis perpendicular to the substrate surface [16]. Figure 1 shows the (002) peaks of the CZO films at approximately 34°. CZO film compositions were analyzed by EDS. CZO films varied in composition as a function of increased dc power applied to the Ce target.
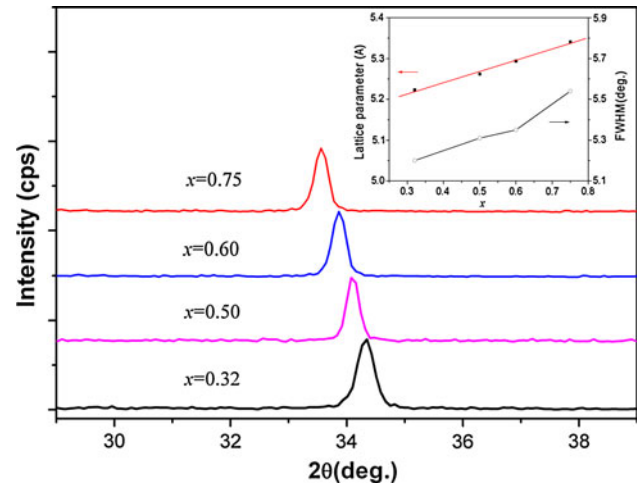

Fig. 1 Expanded XRD θ–2θ patterns at approximately 34° of Ce$_x$Zr$_{1-x}$O$_2$ (002) peak. The *insert* shows lattice parameters and the FWHM values

The values for the atomic fraction (x) were approximately 0.32, 0.5, 0.6, and 0.75 when Ce target power was 30, 50, 75, and 100 W, respectively. From Fig. 1, a clear shift of the (002) peak position towards a lower diffraction angle shows an increase in lattice spacing with increasing Ce concentration. The increase is a result of Ce^{4+} (1.11 Å) having a larger effective ionic radius than Zr^{4+} (0.86 Å). The lattice parameters that changed with Ce fraction were calculated from these XRD data, shown in the insert. A linear dependence of the lattice parameter with x is observed. With a 45° rotation of CZO with respect to the NiW, the lattice mismatch between CZO and NiW varies from 7.8% (Ce$_x$Zr$_{1-x}$O$_2$ with $x = 0.75$) to 4.9% (Ce$_x$Zr$_{1-x}$O$_2$ with $x = 0.32$). Furthermore, the insert shows the full

Fig. 2 Typical SIMS analysis on a Ce$_{0.32}$Zr$_{0.68}$O$_2$/NiW structure showing a sharp interface

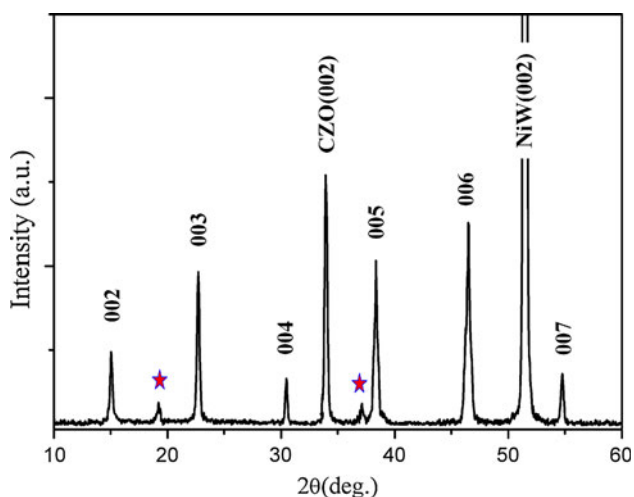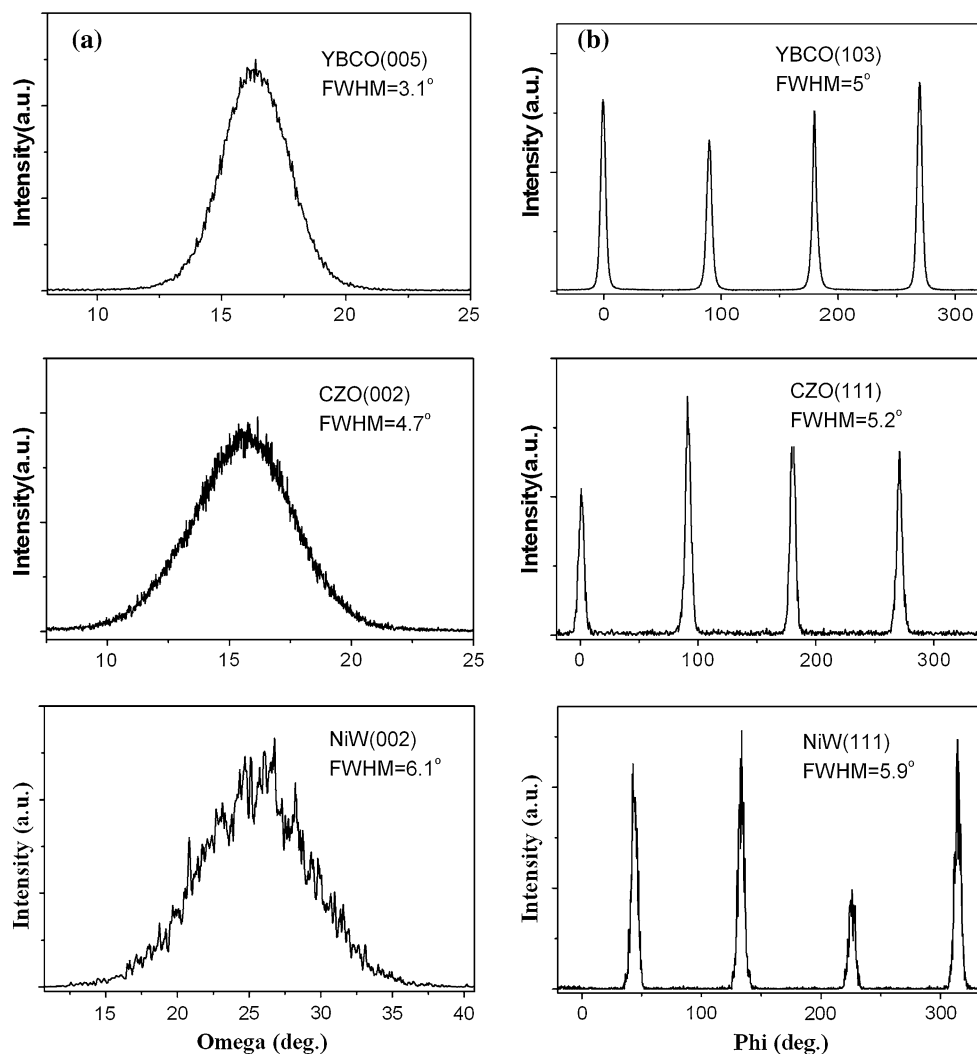**Fig. 3** Typical XRD θ–2θ pattern of the YBCO films on $Ce_{0.32}Zr_{0.68}O_2$/NiW substrate. Weak $NiWO_4$ and NiO impurity peaks are denoted by *stars*

width at half maximum (FWHM) values of CZO (002) diffraction peaks. FWHM values increased with Ce concentration, indicating that crystal quality became worse, which attributed to the stress in the CZO films. Overall, the increase in Ce content correlates with an increase in compressive stress induced by the mismatch between CZO and substrate, which would result in deterioration of the crystalline quality of the CZO films. Therefore, $Ce_{0.32}Zr_{0.68}O_2$ was used as the single buffer layer for the subsequent YBCO CCs.

Usually, a careful control of the different surface and interface is required to achieve the desired epitaxy. A typical AFM micrograph of the surface morphology for 0.3 μm-thick $Ce_{0.32}Zr_{0.68}O_2$ film exhibits a continuous, crack-free, and dense surface morphology, with an average roughness of 3.3 nm [16]. To investigate the ability of the buffer layer to block the diffusion of metal elements, especially Ni and W from the substrate, SIMS depth

Fig. 4 a out-of-plane (ω-scans) and **b** in-plane (ϕ-scans) texture for YBCO film on $Ce_{0.32}Zr_{0.68}O_2$/NiW substrate

profile analyses were performed (shown in Fig. 2). The measurement of the sputter depth profile shows a sharp interface between the substrate and the buffer layer.

The performance of the reactively sputtered $Ce_{0.32}Zr_{0.68}O_2$ buffer layers was evaluated by depositing 0.54 μm YBCO layers. A typical XRD θ–2θ scan of the YBCO film is shown in Fig. 3. The YBCO film exhibits excellent c-axis orientation. Weak $NiWO_4$ and NiO impurity peaks (denoted by stars) are observed at around 19° and 37°, respectively, implying minor oxidation of the metal substrate interface. The relative out-of-plane and in-plane textures for YBCO films on 0.3 μm-thick $Ce_{0.32}Zr_{0.68}O_2$ buffered NiW substrates are documented in Fig. 4a and b, respectively. The ω-scans (Fig. 4a) obtained from the reflections of (002) NiW (002) $Ce_{0.32}Zr_{0.68}O_2$ and (005) YBCO, yield peak-width FWHM values ($\Delta\omega$) of 6.1°, 4.7°, and 3.1°, respectively, indicating good out-of-plane crystallographic alignment among the layers. In-plane textures of the individual layers for the same sample are illustrated in Fig. 4b, where ϕ-scans of (111) NiW, (111) $Ce_{0.32}Zr_{0.68}O_2$, and (103) YBCO reveal four equally spaced peaks, with in-plane FWHM values ($\Delta\phi$) of 5.9°, 5.2°, and 5.0°, respectively, indicating a significant improvement in the in-plane and out-of-plane textures. The epitaxial relationship between YBCO, $Ce_{0.32}Zr_{0.68}O_2$, and NiW can be summarized as $(001)_{YBCO}\|(001)_{Ce0.32Zr0.68O2}\|(001)_{NiW}$ and $[100]_{YBCO}\| [110]_{Ce0.32Zr0.68O2}\|[100]_{NiW}$.

The superconducting performance of YBCO film was assessed by transport measurements. T_c and self-field J_c were 90.4 K and 1.3 MA/cm^2, respectively. In-field transport studies were conducted as well. Figure 5 shows field-dependent J_c versus applied field at 75.5 K with the magnetic field parallel to the YBCO c axis (H||c). The exponent α in the relation $J_c \sim H^{-\alpha}$ was determined to be 0.6 for

this sample as compared to the typical value of 0.5–0.6 for pure PLD-YBCO films. The inset shows the angular dependence of J_c at 75.5 K and 1 T, with the field always in the maximum Lorentz force configuration. The variation of J_c with field orientation or angle (H||ab) is expected due to the intrinsic anisotropy of the YBCO films from the layered CuO planes, or the pinning defects aligned with the ab-planes, such as in stacking faults [17]. Also, the much broader peak for H||c is observed to be attributable to c axis-correlated defects in this film, such as threading dislocations, twin boundaries, and grain boundary dislocations. These results indicate good superconducting behaviors similar to standard CeO_2/YSZ/CeO_2 multilayer buffered samples [18].

Conclusions

We have demonstrated that CZO films were obtained by reactive co-sputtering of Ce and Zr metal targets on biaxially textured metal substrates. The CZO lattice parameter can be tailored from 5.22 to 5.34 Å by changing the composition. The epitaxial YBCO films grown on the 0.3 μm-thick $Ce_xZr_{1-x}O_2$ single buffer layer have a T_c of 90.4 K and J_c (75.5 K, self field) of 1.3 MA/cm^2. The in-field behavior indicates that superconducting samples are as good as those on CeO_2/YSZ/CeO_2 multi-buffer layers. This simple buffer architecture will reduce manufacturing costs and process easily in the production of YBCO CCs.

Fig. 5 J_c versus applied magnetic field for YBCO films on $Ce_{0.32}Zr_{0.68}O_2$/NiW substrate. The *inset* shows the angular dependence of J_c at 75.5 K and 1 T

References

1. Norton DP, Goyal A, Budai JD, Christen DK, Kroeger DM, Specht ED, He Q, Saffian B, Paranthaman M, Klabunde CE, Lee DF, Sales BC, List FA (1996) Science 274:755
2. Maiorov B, Baily SA, Zhou H, Ugurlu O, Kennison JA, Dowden PC, Holesinger TG, Foltyn SR, Civale L (2009) Nat Mater 8:398
3. Matsumoto K, Mele P (2010) Supercond Sci Technol 23:014001
4. Goyal A, Norton DP, Budai JD, Paranthaman M, Specht ED, Kroeger DM, Christen DK, He Q, Saffian B, List FA, Lee DF, Martin PM, Klabunde CE, Hartfield E, Sikka VK (1996) Appl Phys Lett 69:1795
5. Xiong J, Tao BW, Qin WF, Tang JL, Han X, Li YR (2008) Supercond Sci Technol 21:025016
6. Shi DQ, Ko RK, Song KJ, Chung JK, Ha HS, Kim HS, Moon SH, Yoo SI, Park C (2005) Supercond Sci Technol 18:561
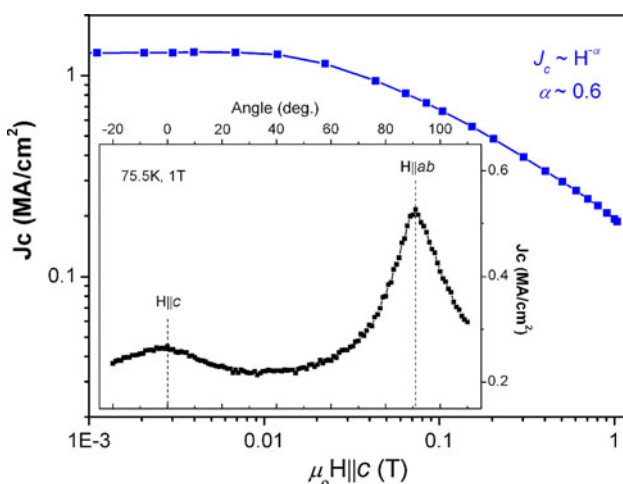7. Kim HS, Park C, Ko RK, Shi DQ, Chung JK, Ha HS, Park YM, Song KJ, Youm DJ (2005) Physica C 426–431:926

8. Ying LL, Lu YM, Liu ZY, Fan F, Gao B, Cai CB, Thersleff T, Reich E, Hühne R, Holzapfel B (2009) Supercond Sci Technol 22:095005

9. Paranthaman MP, Aytug T, Kang S, Feenstra R, Budai JD, Christen DK, Arendt PN, Stan L, Groves JR, DePaula RF, Foltyn SR, Holesinger TG (2003) IEEE Trans Appl Supercond 13:2481

10. Aytug T, Paranthaman M, Kang S, Zhai HY, Leonard KJ, Vallet CE, Sathyamurthy S, Christen HM, Goyal A, Christen DK (2003) IEEE Trans Appl Supercond 13:2661

11. Dawley JT, Ong RJ, Clem PG (2002) J Mater Res 17:1678

12. Paranthaman M, Goyal A, List FA, Specht ED, Lee DF, Martin PM, He Q, Christen DK, Norton DP, Budai JD, Kroeger DM (1997) Physica C 275:266

13. Xiong J, Chen Y, Qiu Y, Tao B, Qin W, Cui X, Tang J, Li Y (2006) Supercond Sci Technol 19:1068

14. Xiong J, Qin W, Cui X, Tao B, Tang J, Li Y (2007) J Cryst Growth 300:364

15. Xiong J, Qin W, Cui X, Tao B, Tang J, Li Y (2006) Physica C 442:124

16. Xiong J, Tao BW, Qin WF, Feng X, Song XK, Zhang F, Li YR (2009) J Phys Conf Ser 153:012036

17. Schilling A, Fisher RA, Phillips NE, Welp U, Dasgupta D, Kwok WK, Crabtree GW (1996) Nature 382:791

18. Varanasi CV, Burke J, Brunke L, Lee JH, Wang H, Barnes PN (2009) IEEE Trans Appl Supercond 19:3152